ARID ZONE JOURNAL OF ENGINEERING, TECHNOLOGY & ENVIRONMENT
AZOJETE June 2026. Vol.22(2):340-350
Published by the Faculty of Engineering, University of Maiduguri, Maiduguri, Nigeria.
Print ISSN: 1596-2490, Electronic ISSN: 2545-5818
https://doi.org/10.63958/AZOJETE/2026/22/02/012
www.azojete.com.ng

ORIGINAL RESEARCH ARTICLE

DESIGN AND DEVELOPMENT OF RECONFIGURABLE PMSM FOR STATOR WINDING TURN VARIATION INVESTIGATION

B. O. Akinloye, F. Tanshi, G. O. Jemiriayigbe*

Department of Electrical and Electronics Engineering, Federal University of Petroleum Resources, Effurun, Delta State 330102. Nigeria
**Corresponding author's email: omatsej@yahoo.com*

ARTICLE INFORMATION

Received: 27th February 2026
Revised: 27th April 2026
Accepted: 28th April 2026

Keywords:
Permanent magnet synchronous motor
Stator winding turns
Electromagnetic module
Torque characteristics
Finite element analysis
Multitap winding

ABSTRACT

Permanent Magnet Synchronous Motors (PMSMs) play a central role in modern industries due to their high efficiency and torque density; however, experimental platforms that allow controlled variation of key electromagnetic parameters—particularly stator winding turns—are limited. This paper presents the design, development, and experimental validation of an electromagnetic module based on a laboratory-scale permanent magnet synchronous motor developed to investigate the influence of stator winding variation on torque characteristics. The research integrates analytical design, finite-element simulation, and controlled laboratory experimentation. A permanent magnet synchronous motor prototype was designed from first principles, covering magnetic loading, induced EMF, conductor sizing and winding distribution. A multitap stator winding arrangement was implemented, enabling the effective number of turns to be varied between 40 and 60 without physical rewinding. Finite-element model was developed using ANSYS to predict electromagnetic torque behavior, while experimental tests were conducted using an inverter-fed drive system. Simulation results revealed a non-monotonic torque response, with torque peaking at intermediate winding configurations, 23.29 Nm at 45 turns, before decreasing at higher turn counts, indicating the influence of electrical and magnetic constraints captured within the numerical model. In contrast, experimental measurements showed a stronger torque dependence on winding configuration, with torque increasing from 22.81 Nm at 40 turns to a maximum of 28.94 Nm at 55 turns, followed by a slight reduction to 27.27 Nm at 60 turns. The results confirm that stator winding variation is a dominant but multi-dimensional design parameter in permanent magnet synchronous motor torque performance and that optimal torque occurs within a finite winding range rather than through indefinite turn increase. The developed electromagnetic module serves as a flexible experimental platform for parametric studies in electric machine design, optimization and education.

1.0 Introduction

Electric motors have been the bedrock of industrial development since the early 19th century when Michael Faraday developed the first crude electric motor in 1821, demonstrating the principle of electromagnetic induction that remains fundamental to motor action (Al-Khalili, 2015). Among the various motor types developed, the permanent magnet synchronous motor (PMSM) has gained significant attention due to its high-power density, superior efficiency, compact, high power factor and better controllability (Umoh *et al.*, 2025).

PMSMs are increasingly used in electric vehicles, robotics, renewable energy systems, and aerospace applications because they eliminate the need for external excitation and brushes, reducing energy losses

and maintenance requirements (Basappa & Viswanathan, 2022). The stator winding configuration, particularly the number of turns, is one of the most critical determinants of motor performance. The winding arrangement interacts closely with other key design parameters such as air-gap length and excitation level, together exerting significant influence on the motor's speed-torque behavior (Manu, 2021).

Despite extensive research on PMSM optimization, significant efforts have primarily focused on machine geometry, electromagnetic performance, and control strategies with Umoh *et al.* (2025) optimizing PMSM electromagnetic design parameters including air gap, rotor dimensions, and pole embrace to improve efficiency and reduce machine size. Similarly, Chen and Lee (2019) conducted finite-element-based sensitivity analysis of rotor geometrical parameters in V-shaped IPMSMs to enhance torque, efficiency, and flux-weakening capability. Sun *et al.* (2019) further investigated PMSM optimization for electric vehicle applications through air-gap, magnet structure, and stator geometry refinement to reduce torque ripple and thermal effects. In the area of control systems, Thampi (2019) reviewed advanced PMSM control strategies aimed at improving speed regulation and dynamic response under varying operating conditions. More recently, Bian and Chien (2025) developed an adaptive fractional-order sliding mode controller to improve robustness and disturbance rejection in PMSM drives. Machine configuration and winding structures have also received considerable attention, with Qiu *et al.* (2020) comparing concentrated and distributed windings in PMSMs using finite-element analysis and experimental validation, while Liu *et al.* (2021) proposed permanent magnet optimization methods for reducing air-gap flux harmonics and improving electromagnetic performance. However, despite these advances, a critical limitation persists in both academic research and industrial development: the lack of experimental platforms that enable controlled variation of key electromagnetic design parameters, particularly stator winding turn count.

Within the broader context of parameter sensitivity in PMSMs, previous studies have extensively analyzed the influence of air gaps surrounding permanent magnets and the role of flux concentrators in PMSMs with internal magnetic circuits as presented by Szewczyk *et al.* (2011), Cha *et al.* (2025) and Guidotti *et al.* (2025). Ulum *et al.*, (2025) demonstrated that reducing the air gap length generally enhances magnetic coupling torque output but increases sensitivity to mechanical tolerances. Lee (2018) presented a comprehensive stability analysis of deadbeat-direct torque and flux control for interior PMSM drives with respect to machine parameter variations, while Kumar *et al.*, (2019) explored the design and modeling of five-phase PMSGs for wind power applications using Dynamic Reluctance Network Modeling. Further investigations into machine structure and configuration have also highlighted the sensitivity of PMSM performance to winding and topology choices. Boztas *et al.*, (2020) applied multi-objective Genetic Algorithm optimization for high power density PMSM design, while Lim *et al.*, (2022) investigated tap-change PMSMs for electric vehicle applications, their work focused on discrete turn ratios for efficiency optimization rather than comprehensive torque characterization. Similarly, Cui *et al.*, (2020) explored asymmetric windings but did not conduct parametric studies of turn variation effects.

As highlighted earlier, while extensive work exists on parametric, control strategy and structural optimization for PMSMs, systematic experimental investigation of stator winding turn variation remains insufficiently explored. This research addresses this gap by designing and developing an electromagnetic module, a specialized PMSM, that enables controlled and repeatable adjustment of stator winding turns within a single integrated system. The module incorporates a multitap winding arrangement allowing variation from 40 to 60 turns, enabling systematic investigation of the relationship between winding configuration and torque output. The research integrates analytical design, finite-element simulation, and experimental validation to provide comprehensive insights into turn-dependent performance characteristics.

2. Materials and Method

The motor was designed as a three-phase, four-pole PMSM with twenty-four stator slots, targeting 500W output power at 380VAC, 50Hz supply. The stator structure employs transparent cast acrylic (PMMA), prioritizing educational visualization of internal electromagnetic components, despite sacrificing approximately 40-60% electromagnetic performance compared to equivalent steel-core designs. This non-magnetic structure ($\mu_r \approx 1.0$) eliminates core flux paths and saturation effects, simplifying magnetic circuit analysis while enabling direct visual observation during operation. The acrylic provides adequate mechanical strength (tensile strength 69 MPa), acceptable thermal performance (maximum service temperature 82°C), excellent machinability for laboratory fabrication, and low cost (~$50 for stator material).

Corresponding author's email address: omatsej@yahoo.com

The rotor core utilizes polyvinyl chloride (PVC) selected for non-magnetic properties ($\mu_r \approx 1.0$), good machinability enabling precision mounting flats for magnets, adequate mechanical strength for 1500 rpm operation. Four NdFeB N42 grade permanent magnets (46×8×2.6mm dimensions,B_r = 1.28T) provide rotor field excitation, selected for high remanence enabling adequate flux density (~0.75T air gap) while maintaining reasonable cost and commercial availability. The 20mm diameter aluminum alloy shaft (6061-T6) offers sufficient strength, low weight, good machinability, and non-magnetic properties.

Stator windings employ AWG 22 enameled copper wire (0.644mm bare diameter, 0.33mm² cross-sectional area) selected to accommodate calculated current density while enabling hand-winding with adequate flexibility for tap extraction and routing to external terminal blocks. The multitap configuration incorporates five connection points (40, 45, 50, 55, 60 turns per slot) extracted during winding and routed to three 9-pin terminal blocks mounted on the base plate.

Sealed deep-groove ball bearings support the rotor shaft, selected for adequate load rating, speed rating, integrated rubber seals preventing contamination and standard dimensions enabling straightforward procurement and replacement.

This material selection balances competing requirements: educational accessibility through visual transparency and conventional fabrication methods, adequate electromagnetic performance for parametric torque characterization, thermal safety with passive cooling and economic feasibility with total material cost of $324 enabling multi-institutional adoption.

2.1 Output Equations

The fundamental motor specifications were established based on research objectives and functional requirements. Key electromagnetic loading specifications include magnetic loading of 0.8T, electric loading of 8kA/m, current density of 4A/mm², flux coefficient factor of 0.89, and winding factor of 0.7.

The output equations governing the motor's electromagnetic performance were derived from fundamental principles. The induced EMF per phase is expressed as:

$$E_{ph} = 4.44 * f * \varphi_p * T_{ph} * k_w \text{ (Wan } et\ al., 2018) \quad 1$$

where f is frequency, φ_p is air gap flux per pole, T_{ph} is number of turns per phase, and k_w is the winding factor.

The magnetic loading is given by:

$$B_g = \frac{P * \varphi_p}{\pi * \mathrm{D}_{\boldsymbol{si}} * L} \text{(Aghazadeh } et\ al., 2019) \quad 2$$

where $\mathrm{D}_{\boldsymbol{si}}$ is the internal stator diameter and L is the core length.

The developed power P can be expressed as:

$$P = 11 * {\mathrm{D}_{\boldsymbol{si}}}^2 * B_g * A_c * L * N_s * k_w * 10^{-3} kva \text{(Aghazadeh } et\ al., 2019) \quad 3$$

where $A_c$is electric loading and N_s is synchronous speed.

The output coefficient of the motor is:

$$C_O = \pi^2 * B_g * A_c * 10^{-3} \text{(Aghazadeh } et\ al., 2019) \quad 4$$

2.2 Multitap Winding Design

The multitap winding system was designed to enable variation of effective turns without physical rewinding. The turns per slot was calculated using:

$$T_s = \frac{T_{ph} * m}{Q} (Izanlo\ et\ al., 2020) \quad 5$$

Corresponding author's email address: omatsej@yahoo.com

where T_s is turns per slot, Q is total slots, and m is number of phases. With 60 turns per slot as the maximum configuration, tap points were established at 55, 50, 45, and 40 turns, corresponding to 92%, 83%, 75%, and 67% configurations respectively.

The conductor cross-sectional area was determined from current density requirements:

$$A_c = \frac{I_{ph}}{J} (Tun \ \& \ Tin, 2014) \quad 6$$

where I_{ph} is phase current and J is current density. AWG 22 copper wire with 0.33mm² cross-sectional area was selected.

2.3 Stator and Rotor Design

The stator was constructed from acrylic (Perspex) material to provide transparency for educational visualization while maintaining structural integrity. The stator internal diameter (D_{sI}) and core length (L) were determined from:

$$D_{sI}{}^2 * L = \frac{P}{C_O * N_s} (Tun \ \& \ Tin, 2014) \quad 7$$

The aspect ratio (core length to pole pitch) was selected as 1.2, yielding a stator internal diameter of 80mm and core length of 100mm.

The rotor was constructed from PVC material with neodymium magnets arranged in a four-pole configuration. The rotor outer diameter was calculated accounting for air gap length:

$$D_{ro} = D_{si} - 2g \ (Oduyemi \ \& \ Chibueze, 2020) \quad 8$$

where $D_{ro}$is the diameter of the rotor, g is the air gap length (1mm), resulting in a rotor diameter (D_{ro}) of 78mm.

2.4 Control System

A vector frequency inverter was implemented to provide variable voltage and frequency control. The V/f control strategy maintains constant air-gap flux by preserving the voltage-to-frequency ratio:

$$\frac{V}{f} = constant \ (Strulrajter \ et \ al., 2007) \quad 9$$

Sinusoidal pulse width modulation (SPWM) was employed to synthesize the three-phase AC output, with the synchronous speed controlled according to:

$$n_s = \frac{120f}{p} (Hanselman, 2006) \quad 10$$

where p is the number of poles.

2.5 ANSYS Modeling

Finite-element models were developed using ANSYS Maxwell to predict electromagnetic behavior. The 3D models incorporated the physical parameters obtained from the analytical calculations, as shown in Table 1. Boundary conditions included flux-parallel outer stator surfaces and periodic symmetry exploitation. The air gap region was meshed with 0.2mm element size for accurate flux density gradient resolution. Figure 1 displays the flux lines of the model, indicating the magnetic field distribution within the motor.

2.6 System Integration

System integration assembled designed components into a functional electromagnetic module through mechanical assembly, electrical connections, and operational verification.

The acrylic stator was secured to the 610×610×10 mm base frame with the rotor assembly (PVC core, NdFeB magnets, aluminum shaft) inserted maintaining uniform 1 mm air gap. Pillow block bearings provided

Corresponding author's email address: omatsej@yahoo.com

rotational support and alignment. The multitap stator windings were terminated at five tap points (40, 45, 50, 55, 60 turns per slot) routed to three 9-pin terminal blocks enabling reconfiguration without disassembly. Three-phase windings connected in star configuration interfaced with a vector frequency inverter through circuit breaker protection. Figure 2 shows the complete electromagnetic module assembly as modeled in SolidWorks. Plate I illustrates the physical electromagnetic module.

Table 1: Physical Parameters of the Electromagnetic Module

Parameter	**Value**
Number of Phases	3
Number of Poles	4
Number of Slots	24
Stator Inner Diameter	80 mm
Core Length	100 mm
Air Gap Length	1 mm
Rotor Outer Diameter	78 mm
Conductor Size	AWG 22
Turns per Slot (max)	60
Rated Power	500 W
Rated Voltage	380 VAC
Rated Frequency	50 Hz

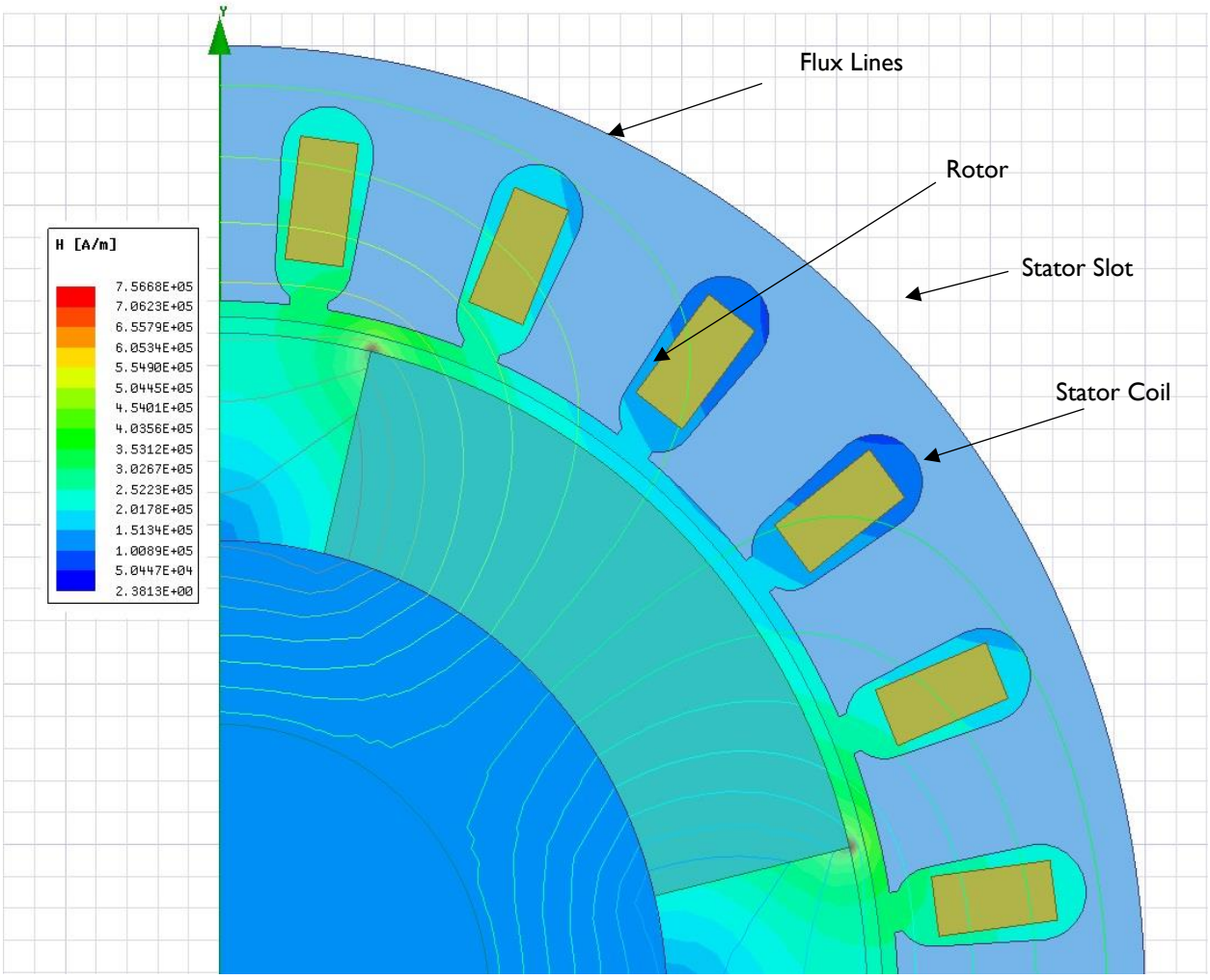

Figure 1: Flux line representation on the ANSYS model of the PMSM

Corresponding author's email address: omatsej@yahoo.com

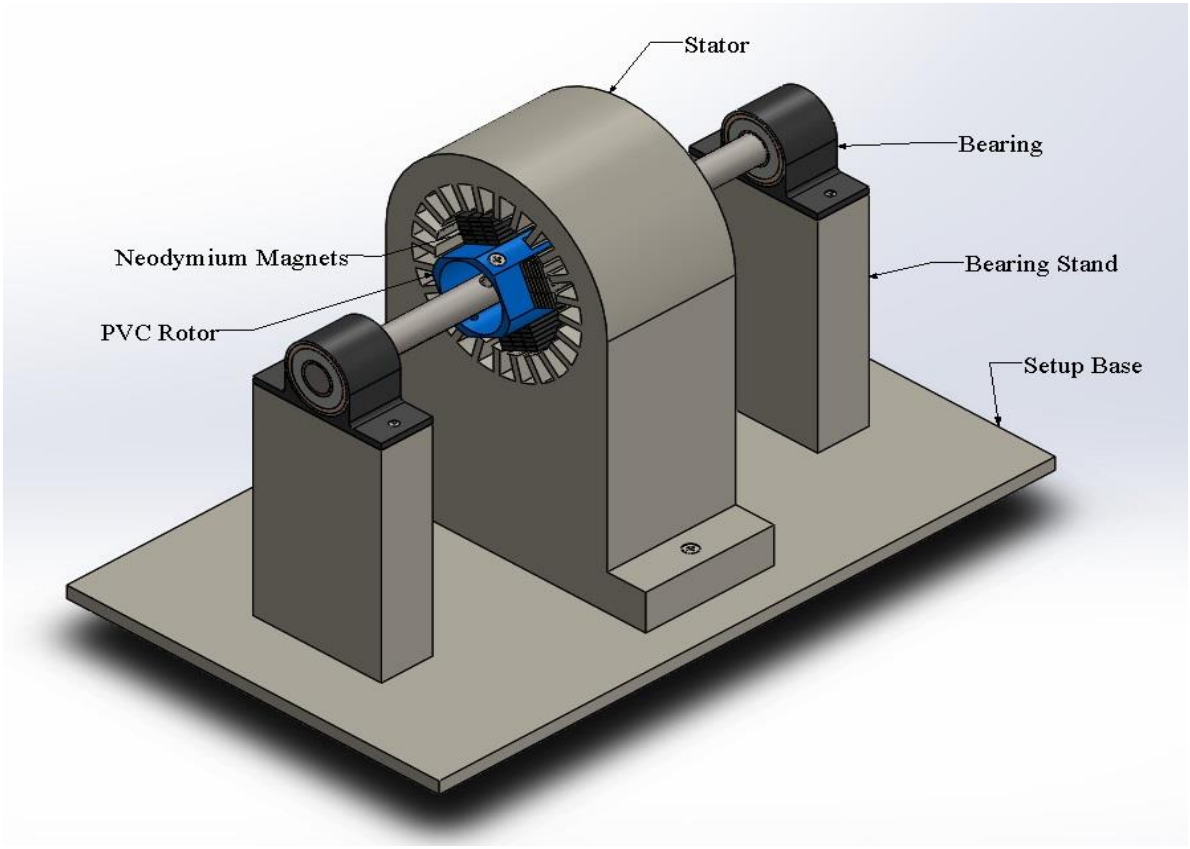

Figure 2: SolidWorks representation of the electromagnetic module

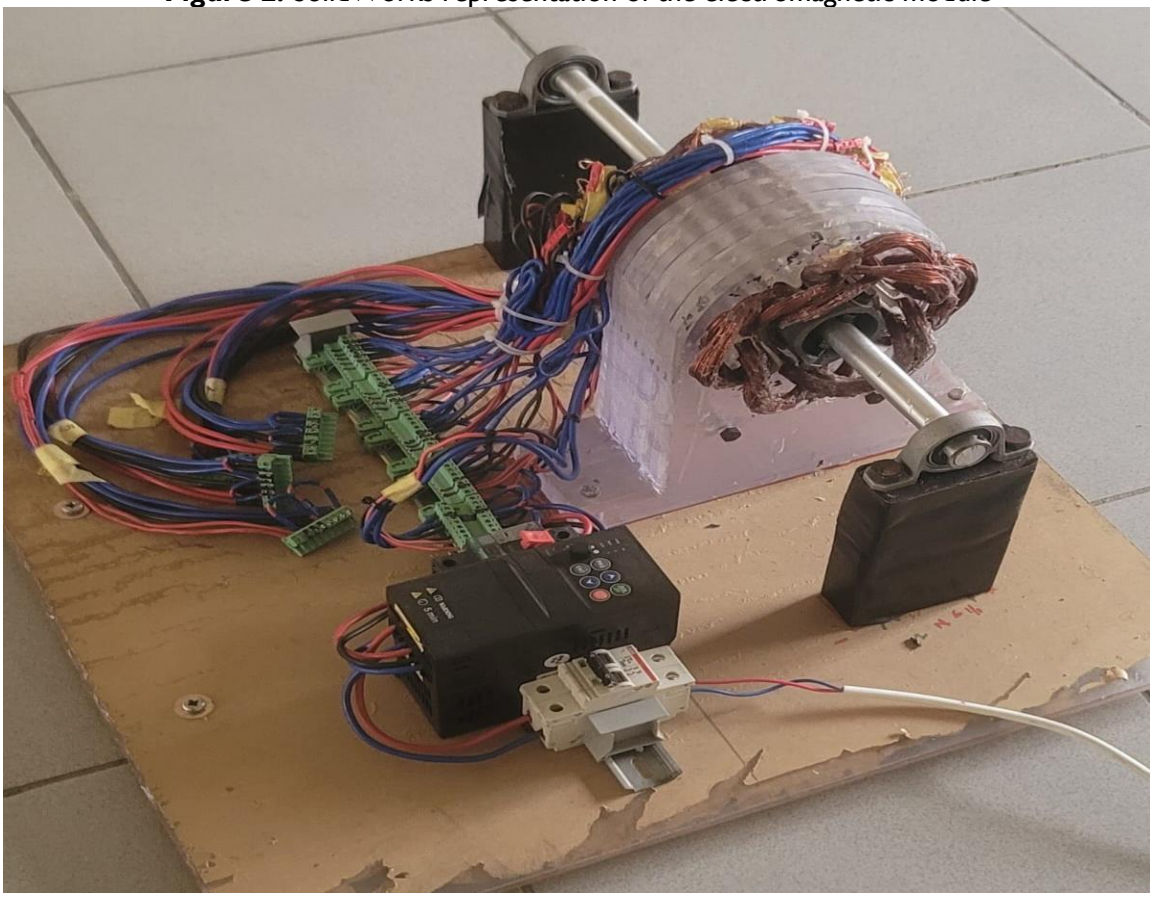

Plate 1: The physical electromagnetic module

3. Results and Discussion

Experimental and simulation investigations were conducted for five stator winding configurations of 40, 45, 50, 55, and 60 turns in order to evaluate the influence of turn variation on PMSM torque characteristics. Finite-element predictions were obtained using ANSYS Maxwell simulations, while experimental torque values were determined from measured electrical power and rotational speed using Equation 11.

Corresponding author's email address: omatsej@yahoo.com

$$T = \frac{P}{n} = \frac{\sqrt{3} * V * I * \eta}{(2 * \pi * f)/60} \ (Chapman, 2012) \quad 11$$

3.1 Simulated Torque Performance at Different Turn Configurations

Finite element simulation was carried out using design parameters for the electromagnetic module under constant speed and varying speed operating conditions. The simulation results are presented in Table 2.

Table 2: ANSYS Simulation Results for Turn Variation

Turns	Torque @ 1500 rpm (Nm)	Torque @ Variable Speed (Nm)
60	4.7978	22.14 @ 325rpm
55	4.5825	22.61 @ 304rpm
50	4.3352	22.74 @ 286rpm
45	4.0526	23.29 @ 261rpm
40	3.7327	22.95 @ 244rpm

The ANSYS Maxwell simulation results revealed that torque output varied with stator winding turn count, although the variation remained relatively moderate compared with experimental observations. Under constant-speed conditions at 1500 rpm, the predicted torque increased progressively from 3.7327 Nm at 40 turns to 4.7978 Nm at 60 turns. Under variable-speed operating conditions, however, the highest torque (23.29 Nm) occurs at 45 turns, indicating that maximum turn count did not correspond to optimal torque output. This shows that excessive stator turns mean increased electrical impedance that negatively impacts torque performance. To visualize the relationship between torque and stator turns, the simulated results are plotted in Figure 3

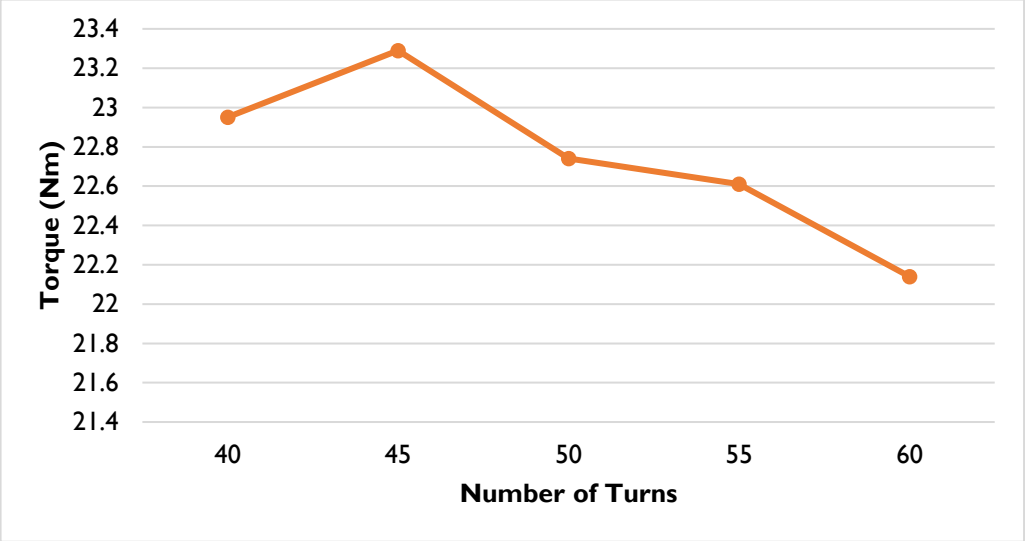

Figure 3: Graph of torque output on ANSYS vs number of turns

The graph shows a non-linear torque pattern, with peak performance at intermediate turns (45 turns) rather than at the highest turn setting. This demonstrates that optimum winding design requires balancing magnetic flux gain against winding impedance.

3.2 Experimental Torque Performance at Different Turn Configurations

Experimental tests were conducted for the same five winding configurations. The number of stator turns was varied progressively by reducing the initial sixty turns in steps of five turns, down to forty turns per slot. To be able to obtain the experimental torque, the current drawn by the windings and the rotor speed were measured.

Corresponding author's email address: omatsej@yahoo.com

3.2.1 Experimental running current at different turn configurations

For each winding configuration, at a voltage of 380VAC, the average running currents were recorded as shown in Table 3.

Table 3: Experimental Running Current at Different Turn Configurations

Turns	Average Running Current (A)
60	2.20
55	2.19
50	1.96
45	1.65
40	1.38

The running current increased with increase in stator turns. Higher turns required greater electrical loading under the test condition, thus suggesting that winding impedance and power demand became more significant at larger turn counts.

3.2.2 Experimental Running Speed at Different Turn Configurations

The running speed of the developed PMSM was measured for each turn configuration and is presented in Table 4.

Table 4: Experimental Running Speed at Different Turn Configurations

Turns	Average Running Speed (rpm)
60	325
55	304
50	286
45	261
40	244

The rotor speed increased progressively with increasing turns. This indicates that improved induced EMF and stronger electromagnetic coupling at higher turn counts enhanced rotational performance.

3.2.3 Experimental Torque Determination at Different Turn Configurations

Using the measured speed, current and voltage data, experimental torque was calculated using Equation 11. The results are shown in Table 5 and are compared with the simulated torque performance values.

Table 5: Comparison of Simulated and Experimental Torque Values

Turns	Simulated Torque (Nm)	Experimental Torque (Nm)
60	22.14	27.27
55	22.61	28.94
50	22.74	27.50
45	23.29	25.42
40	22.95	22.81

The experimental results revealed stronger dependence of torque on winding turns than predicted by simulation. Torque increased from 22.81 Nm at 40 turns to 25.42 Nm at 45 turns and further to 27.50 Nm at 50 turns. The maximum measured torque of 28.94 Nm occurred at 55 turns, after which the torque

Corresponding author's email address: omatsej@yahoo.com

reduced slightly to 27.27 Nm at 60 turns. The increase in torque between 40 and 55 turns confirms that increasing turns improved stator flux linkage and strengthened magnetic flux coupling with the rotor magnets. However, the reduction observed at 60 turns indicates the onset of limiting effects such as higher copper losses, increased resistance and greater inductive reactance. Both simulation and experimental investigations confirm that torque performance is highly dependent on stator winding turns. The combined torque behavior is illustrated in Figure 4

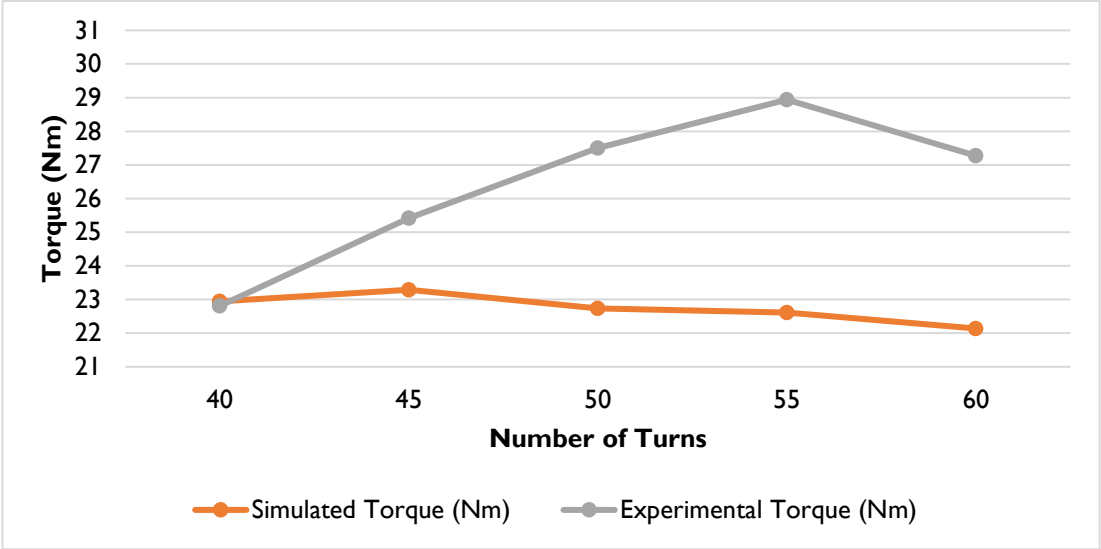

Figure 4: Graph of torque (experimental and simulated) vs number of turns

The graph clearly shows that experimental torque increased significantly up to 55 turns before declining slightly, while simulated torque remained relatively stable across the tested range. Both results confirm that optimum torque occurs within a finite turn range rather than through indefinite turn increase. However, some differences were observed between the predicted and measured torque performances. The simulation identified 45 turns as the optimum configuration with a peak torque of 23.29 Nm, whereas the experimental system achieved maximum torque at 55 turns with a substantially higher value of 28.94 Nm.

The consistently higher experimental torque values suggest that practical machine behavior included beneficial effects not fully captured in the finite-element model. These may include three-dimensional fringing flux, end-winding magnetic interaction, local flux concentration, and real inverter operating dynamics. In addition, slight material and assembly variations may influence current distribution and torque production.

The shift in optimum turn count from 45 turns in simulation to 55 turns experimentally further demonstrates the importance of physical validation in motor development. While finite-element modeling remains valuable for preliminary design and trend prediction, experimental investigation is necessary to identify the true operating optimum under realistic conditions. Overall, both simulation and experiment confirm that torque performance depends strongly on stator winding turns and that maximum performance occurs within a finite optimal range rather than through indefinite turn increase. The developed electromagnetic module therefore provides an effective platform for studying PMSM winding optimization and validating theoretical design models.

4. Conclusion

This study successfully developed a reconfigurable permanent magnet synchronous motor (PMSM)-based electromagnetic module for investigating the effect of stator winding turn variation on torque performance. The multitap winding arrangement enabled controlled adjustment of the effective turns from 40 to 60 without repeated rewinding, providing a practical platform for systematic experimental analysis.

Analytical design methods, finite-element simulation, and experimental testing were employed to determine the motor characteristics and evaluate the influence of winding turn variation on torque output. Both simulation and practical results confirmed that stator winding turn count significantly affects PMSM performance and that optimum torque occurs within an intermediate range rather than through continuous increase in turns. The experimental investigation showed that torque increased from 22.81 Nm at 40 turns

Corresponding author's email address: omatsej@yahoo.com

to a peak value of 28.94 Nm at 55 turns, before declining slightly to 27.27 Nm at 60 turns, thereby identifying 55 turns as the optimal configuration under the tested conditions.

Overall, the findings demonstrate that stator winding turn count is a critical but non-monotonic PMSM design variable. Maximum torque is achieved within a finite optimal range rather than by simply increasing the number of turns. The developed module therefore provides a useful platform for electric machine education, design optimization, and future investigations involving efficiency improvement, thermal analysis, and advanced motor control strategies.

REFERENCES

Aghazadeh, H., Afjei, E. and Siadatan, A. 2019. Sizing and detailed design procedure of external rotor synchronous reluctance machine. IET Electric Power Applications, 13(8): 1105–1113. https://doi.org/10.1049/iet-epa.2018.5802.

Al-Khalili, J. 2015. The birth of the electric machines: a commentary on Faraday (1832) 'Experimental researches in electricity.' Philosophical Transactions of the Royal Society a Mathematical Physical and Engineering Sciences, 373(2039): 20140208. https://doi.org/10.1098/rsta.2014.0208

Basappa, MH. and Viswanathan, P. 2022. Various control methods of permanent magnet synchronous motor drives in electric vehicle: a technical review. TELKOMNIKA (Telecommunication Computing Electronics and Control), 20(6): 1225-1229. https://doi.org/10.12928/telkomnika.v20i6.24236

Bian, F. and Chien, Y. 2025. PMSM speed control based on improved adaptive fractional-order sliding mode control. Symmetry, 17(5): 736. https://doi.org/10.3390/sym17050736

Boztaş, G., Yıldırım, M. and Aydogmuş, O. 2020. Design and optimization of a PMSM for obtaining high-power density and high-Speed. Turkish Journal of Science & Technology, 15(2): 61-70 https://izlik.org/JA63MW64UY

Cha, K., Kim, J., Lee, S., and Park, M. 2025. Design of a high-efficiency external rotor interior permanent magnet synchronous motor without magnetic leakage flux path. Mathematics, 13(11): 1865. https://doi.org/10.3390/math13111865

Chapman, SJ. 2012. Electric Machinery Fundamentals. 5th ed., McGraw-Hill, pp. 4, 625.

Chen, H. and Lee, CHT. 2019. Parametric sensitivity analysis and design optimization of an interior permanent magnet synchronous motor. IEEE Access, 7: 159918–159929. https://doi.org/10.1109/access.2019.2950773.

Cui, S., Zhao, T., Du, B. and Cheng, Y. 2020. Multiphase PMSM with asymmetric windings for electric drive. Energies, 13(15): 3765. https://doi.org/10.3390/en13153765

Guidotti, G., Barri, D., Soresini, F., & Gobbi, M. 2025. Optimal design of interior permanent magnet synchronous motor considering various sources of uncertainty. World Electric Vehicle Journal, 16(2): 79. https://doi.org/10.3390/wevj16020079

Hanselman, DC. 2003. Brushless permanent-magnet motor design. Magna Physics Publishing, California, pp. 12. https://digitalcommons.library.umaine.edu/fac_monographs/231

Izanlo, A., Gholamian, SA. and Abdollahi, SE. 2020. Optimal design of a permanent magnet synchronous motor for high efficiency and low cogging torque. International Journal on Electrical Engineering and Informatics, 12(2): 173-186.

Kumar, RR., Singh, S., Srivastava, R. and Saket, R. 2019. Dynamic reluctance air gap modeling and experimental evaluation of electromagnetic characteristics of five-phase permanent magnet synchronous generator for wind power application. Ain Shams Engineering Journal, 11(2): 377–387. https://doi.org/10.1016/j.asej.2019.09.004

Corresponding author's email address: omatsej@yahoo.com

Lee, J. 2018. Stability analysis of deadbeat-direct torque and flux control for permanent magnet synchronous motor drives with respect to parameter variations. Energies, 11(8): 2027. https://doi.org/10.3390/en11082027

Lim, J., Gu, B., Im, S. and Kim, R. 2022. Design of stator winding turn number of tap-change PMSM for EVs according to driving cycles. Energies, 16(1): 412. https://doi.org/10.3390/en16010412

Liu, C., Xu, Y., Zou, J., Yu, G., and Zhuo, L. 2021. Permanent magnet shape optimization method for PMSM air gap flux density harmonics reduction. CES Transactions on Electrical Machines and Systems, 5(4): 284–290. https://doi.org/10.30941/cestems.2021.00033

Manu, PK. 2021. Design and optimization of high-efficiency electric motors. World Journal of Advanced Research and Reviews, 10(2): 282–292. https://doi.org/10.30574/wjarr.2021.10.2.0198

Oduyemi, O. and Chibueze, K. 2020. Imperatives of air-gap length on the performance of electromechanical devices/machines, ResearchGate [Preprint], 15(3): 15-23. https://www.researchgate.net/publication/342436292_Imperatives_of_Air-Gap_Length_on_the_Performance_of_Electromechanical_DevicesMachines.

Qiu, H., Zhang, Y., Yang, C. and Yi, R. 2020. Performance analysis and comparison of PMSM with concentrated winding and distributed winding. Archives of Electrical Engineering, 69(2): 303-317. https://doi.org/10.24425/aee.2020.133027

Stulrajter, M., Hrabovcova, V. and Franko, M., 2007. Permanent magnets synchronous motor control theory. Journal of Electrical Engineering, 58(2): 79–84. https://www.researchgate.net/publication/265347198_Permanent_magnets_synchronous_motor_control_theory

Sun, X. Shi, Z., Lei, G., Guo, Y. and Zhu, J., 2019. Analysis and design optimization of a permanent magnet synchronous motor for a campus patrol electric vehicle. IEEE Transactions on Vehicular Technology, 68(11): 10535–10544. https://doi.org/10.1109/tvt.2019.2939794.

Szewczyk, K., Golisz, R., Walasek, T. and Kucharczyk, Z. 2011. The influence of an air gap around the permanent magnets with the flux concentrator in permanent magnet synchronous motor with internal magnetic circuits. Przeglad Elektrotechniczny, 2011(12b): 181-183. http://pe.org.pl/articles/2011/12b/50.pdf

Thampi, P. and Kiran, C. 2019. A review on controlling techniques for permanent magnet synchronous motor (PMSM) and current state of the art in the Research Area. Communications on Applied Electronics, 7(25): 8–17. https://doi.org/10.5120/cae2019652808

Tun, EKAN. and Tin, T., 2014. Design of conventional permanent magnet synchronous motor used in electric vehicle. International Journal of Scientific Engineering and Technology Research, 3(16): 3289-3293. https://www.academia.edu/81276910/Design_of_Conventional_Permanent_Magnet_Synchronous_Motor_used_in_Electric_Vehicle

Ulum, M., Afandi, AN., Widyaningtyas, T., Haryanto, Fitrahadi A. and Baihaqi, 2025. Influence of flux density, operating frequency, and air gap variation on the rotational performance of PMSM. Proceedings of 2nd Beyond Technology Summit on Informatics International Conference (BTS-I2C), held in Indonesia, IEEE proceedings no. 11399495, 437-441p.

Umoh, GD., Udoakah, YN., and Ekpo, EG., 2025. Design optimization of permanent synchronous motors for improved efficiency using air-gap parametric. Proceeding of the 1st International Conference/Exhibitions of the Department of Mechatronic Engineering, University of Nigeria, Nsukka, 385 - 390.

Wan, Y., Cui, S., Wu, S. and Song, L., 2018. Electromagnetic design and losses analysis of a high-speed permanent magnet synchronous motor with toroidal windings for pulsed alternator. Energies, 11(3): 562. https://www.mdpi.com/1996-1073/11/3/562

Corresponding author's email address: omatsej@yahoo.com